Density fluctuations in molten lithium: inelastic x-ray scattering study

2000 J. Phys.: Condens. Matter 12 8009

(http://iopscience.iop.org/0953-8984/12/37/302)

J. Phys.: Condens. Matter **12** (2000) 8009–8034. Printed in the UK PII: S0953-8984(00)14788-5

Density fluctuations in molten lithium: inelastic x-ray scattering study

T Scopigno†, U Balucani‡, G Ruocco§ and F Sette‖

† Dipartimento di Fisica and INFM, Università di Trento, I-38100, Povo, Italy
‡ Istituto di Elettronica Quantistica CNR, I-50127, Firenze, Italy
§ Dipartimento di Fisica and INFM, Università di L'Aquila, I-67100, L'Aquila, Italy
‖ European Synchrotron Radiation Facility, BP 220, F-38043 Grenoble Cédex, France

Received 16 June 2000

Abstract. New inelastic x-ray scattering experiments have been performed on liquid lithium at two different temperatures: $T = 475$ K (slightly above the melting point) and 600 K. Taking advantage of the absence of any kinematical restriction and incoherent contribution, and pushing the instrumental resolution up to 1.5 meV, it was possible to perform an accurate investigation of the dynamic structure factor $S(Q, E)$ in the wavevector range from 1 to 110 nm^{-1}. For Q smaller than $Q_m \simeq 25$ nm^{-1}, the position of the main peak of the static structure factor, a detailed analysis of the lineshapes shows that any picture of the relaxation mechanisms based on a simple viscoelastic model must be abandoned. All the spectral features can instead satisfactorily be accounted for by including both fast and slow relaxation processes. The physical origin of the slow relaxation is associated with the structural rearrangement, while the local nature of the fast one is extensively discussed. At larger Q-values, a gradual crossover from the strongly correlated to single-particle dynamics occurs, with an important weighting provided by quantum effects.

1. Introduction

The dynamics of liquid metals has been extensively investigated in the recent past with the main purpose of ascertaining the role of the mechanisms underlying both collective and single-particle motions at the microscopic level. In the special case of collective density fluctuations, it is known that well-defined oscillatory modes can be supported even outside the strict hydrodynamic region. In molten alkali metals, this feature is found to persist down to wavelengths of one or two interparticle distances, making these systems excellent candidates for testing the various theoretical approaches developed so far for the microdynamics of the liquid state. As a consequence, since the pioneering inelastic neutron scattering (INS) study by Copley and Rowe [1] on liquid rubidium the interest in performing more and more accurate experiments has been continuously renewed: INS investigations have been devoted to liquid caesium [2], sodium [3], lithium [4], potassium [5] and again rubidium [6].

Up to a few years ago the only experimental probes adequate to access the interparticle distance region in collective dynamics were thermal neutrons. With this technique fundamental results have been achieved in the field of condensed matter structure and dynamics. Unfortunately, in several systems their use for the determination of the dynamic structure factor $S(Q, E)$ becomes extremely difficult (if not impossible) for two reasons. The first one reflects the presence of an incoherent contribution to the total neutron scattering cross section. In liquid sodium, for example, the incoherent cross section dominates; even in more favourable

0953-8984/00/378009+26$30.00

cases (Li, K), at small Q the intensity of the collective contribution is low, and its extraction requires a detailed knowledge of the single-particle dynamics. The second reason is dictated by the need for satisfying both the energy and momentum conservation laws which define the $(Q–E)$ region accessible to the probe [7]. Roughly speaking, when the speed of sound for the system exceeds the velocity of the probing neutrons ($\sim$1500 m s^{-1} for thermal neutrons) collective excitations cannot be detected for Q-values below Q_m, the position of the first sharp diffraction peak of the sample, namely just in the most significant region for the collective properties.

By virtue of the $m^{-1/2}$-dependence of the isothermal speed of sound c_0 (see section 2.1), the higher the atomic number of the system, the wider the kinematic region accessible to neutrons, so accurate INS data are available for rubidium ($c_0 \sim 1260$ m s^{-1}) [1,6] and caesium ($c_0 \sim 970$ m s^{-1}) [2], while more difficulties are met in the case of lighter metals. In particular, lithium represents the most critical case due to its high speed of sound ($c_0 \sim 4500$ m s^{-1}) and to the equality of the coherent and incoherent cross sections: for this reason INS study of collective properties of Li represents a very hard challenge [8]. From a general point of view the main outcome of all these INS experiments, as far as collective properties are concerned, is evidence of inelastic excitations in $S(Q, E)$ that, in the specific cases of rubidium and caesium, exhibit a *positive dispersion*, i.e. an increase of $\omega_m(Q)$ (the position of the $S(Q, \hbar\omega)$ peaks) with respect to the values implied by the hydrodynamic speed of sound. About the details of the relaxations driving such dispersion not much can be inferred at this level: the experimental results have been necessarily analysed within simple models such as the damped harmonic oscillator [6] or the kinetic model [6, 9], suitable to extract reliable and resolution-corrected information on the peak positions but not about the lineshape features. Some extra efforts have been made in the case of caesium where information about an average relaxation time has been extracted [2].

A very useful tool, complementary to the 'traditional' experimental facilities, is the numerical simulation technique, in particular molecular dynamics (MD) simulation: the choice of a realistic interatomic potential—i.e. a potential model able to reproduce structural properties—allows the determination of the dynamics of the system via the integration of the classical Newton equations. In this framework the single-particle and the collective properties can easily be investigated within technical restrictions due to the finite box size (defining the minimum accessible wavevector) and computation time (related to the statistical quality and to the energy resolution of the calculated spectra). Broadly speaking the features of the atomic collective motion, i.e. the details of the $S(Q, E)$ lineshape, as an outcome of the MD run, turn out to be less noisy and more straightforward than the corresponding INS results: no absolute normalizations are required, no mixing between coherent/incoherent dynamics occurs and, above all, basically no resolution corrections are needed.

Since the first experiments on rubidium, a considerable number of MD works have been published in this field, giving valuable support to the experimental measurements [10, 11]. In the specific case of liquid lithium, the MD simulations performed [12, 13] indicate features common to all the other molten alkali metals, like the presence of *positive dispersion*—a particularly relevant result that could have not be achieved with neutrons for the previously mentioned reasons. At temperature around T_m the increase of the velocity of sound is of the order of 20%, and not much is known about its microscopic origin.

In the recent past, the development of new synchrotron radiation facilities opened the possibility of using x-rays to measure $S(Q, \omega)$ (which is proportional to the scattered intensity) in the non-hydrodynamic region; in this case the photon speed is obviously much larger than the excitation velocity, and no kinematic restriction applies. Moreover, in a monatomic system such as lithium, the scattering cross section is purely coherent and so it is directly

associated with the dynamic structure factor. Some experiments have been performed on liquid lithium [14–18] with progressively increasing resolution; it has been possible to show the existence of propagating collective excitations, but due to resolution limitations (never below $\Delta E_{FWHM} \sim 12$ meV), no detailed information about the lineshape could be extracted.

In this work we report the results of inelastic x-ray scattering (IXS) experiments performed on liquid lithium with very high energy resolution, adequate to probe accurately the detailed features of $S(Q, E)$—this allows us to investigate whether the lineshape dependence on momentum transfer can be interpreted within the phenomenology of one or more relaxation processes. In particular in section 2 we review the basic theoretical framework adopted for the interpretation of the IXS results. The latter are reported in section 3 together with a brief account of the experimental set-up. Section 4 is devoted to the data analysis and discussion. The main findings of the present paper are finally summarized in section 5 along with some concluding remarks.

2. Basic theory

2.1. Definitions

In the classical limit, the basic time correlation probing the collective dynamics in a monatomic fluid (N particles with mass m) is the intermediate-scattering function

$$F(Q,t) = (1/N)\sum_{i,j}\left\langle \mathrm{e}^{-\mathrm{i}\boldsymbol{Q}\cdot\boldsymbol{r}_i(0)}\mathrm{e}^{\mathrm{i}\boldsymbol{Q}\cdot\boldsymbol{r}_j(t)}\right\rangle \tag{1}$$

where $\boldsymbol{r}_i(t)$ denotes the position of the jth particle at time t. The dynamic structure factor $S(Q,\omega)$ is the frequency spectrum of $F(Q,t)$, while the structural features are accounted for by the initial value $F(Q,t=0) = S(Q)$. The quantity $F(Q,t)$ then obeys the equation

$$\ddot{F}(Q,t) + \omega_0^2(Q)F(Q,t) + \int_0^t M(Q,t-t')\dot{F}(Q,t')\,\mathrm{d}t' = 0 \tag{2}$$

where

$$\omega_0^2(Q) = K_B T Q^2/mS(Q) \tag{3}$$

is the second classical normalized frequency moment of $S(Q,\omega)$, while $M(Q,t)$ is the so-called memory function of the system, related in some way to the details of the Hamiltonian [19]. In the limit $Q \to 0$, $\omega_0^2(Q) \to c_0^2Q^2$, where c_0 is the isothermal velocity of sound; hence the quantity $c_0(Q) \equiv \omega_0(Q)/Q$ can be interpreted as a suitable generalization of c_0 to finite wavevectors.

From equation (2) a formally exact representation of the Laplace transform of $F(Q,t)$ can be written as [7, 20]

$$\widetilde{F}(Q,z) = \int_0^\infty \mathrm{d}t\ \mathrm{e}^{-zt}F(Q,t) = S(Q)\left\{z+\frac{\omega_0^2(Q)}{[z+\widetilde{M}(Q,z)]}\right\}^{-1}. \tag{4}$$

From the knowledge of $\widetilde{F}(Q,z)$ one straightforwardly obtains

$$S(Q,\omega) = (1/\pi)\,\mathrm{Re}\,\widetilde{F}(Q, z=\mathrm{i}\omega)$$

in terms of the real (M') and imaginary (M'') parts of the Fourier–Laplace transform of the memory function:

$$S(Q,\omega) = \frac{S(Q)}{\pi}\frac{\omega_0^2(Q)M'(Q,\omega)}{\left[\omega^2-\omega_0^2+\omega M''(Q,\omega)\right]^2+\left[\omega M'(Q,\omega)\right]^2}. \tag{5}$$

The spectral features of the dynamic structure factor can be characterized by its frequency moments

$$\Omega_S^{(n)}(Q) \equiv \int \omega^n S(Q,\omega)\,\mathrm{d}\omega$$

where, for a classical system, only the even frequency moments (such as $\Omega_S^{(0)}(Q) = S(Q)$ and $\Omega_S^{(2)}(Q) = S(Q)\omega_0^2(Q)$) are different from zero.

In the following, we shall also find it convenient to consider the 'longitudinal current spectrum' defined as $C_L(Q,\omega) = (\omega^2/Q^2)S(Q,\omega)$. The presence of the factor ω^2 wipes out the low-frequency portion of the dynamic structure factor, and consequently emphasizes the genuine inelastic features of $S(Q,\omega)$. Following from its definition and equation (4), it is readily seen that the Laplace transform $\widetilde{C}_L(Q,z)$ satisfies

$$\widetilde{C}_L(Q,z) = -z[z\widetilde{F}(Q,z) - S(Q)] = \left\{z + [\omega_0^2(Q)/\,z] \;+\; \widetilde{M}(Q,z)\right\}^{-1}. \quad (6)$$

Again, the spectrum $C_L(Q,\omega)$ can be expressed as $(1/\pi)\,\mathrm{Re}\,\widetilde{C}_L(Q, z = \mathrm{i}\omega)$. Then the position and the width of the inelastic peaks in $C_L(Q,\omega)$ are determined by the poles of $\widetilde{C}_L(Q,z)$.

The above definitions are valid for a classical system. In the case of interest to us, the main effect of quantum mechanical corrections stems from the well-known inequality of the positive- and negative-frequency parts of the spectra, connected by the detailed-balance factor $\mathrm{e}^{\beta\hbar\omega}$. Additional sources of non-classical behaviour, such as those associated with a finite value of the de Boer wavelength $\Lambda = (2\pi\hbar^2/mK_BT)^{1/2}$, are small (in the lithium states explored, Λ is only 0.11 times the average interparticle distance) and can safely be neglected. Since the effects of the detailed balance are clearly visible in the experimental IXS spectra, we briefly discuss a possible procedure for accounting for this quantum feature in a consistent way, while preserving the inherent advantages of the classical description. In doing this, for the sake of clarity we shall denote all the previous classical quantities with the subscript *cl*, while the notation q will refer to the quantum case.

The natural theoretical counterpart of the classical density correlation function is the so-called Kubo canonical relaxation function [21]

$$K_q(Q,t) = \frac{1}{\beta N}\sum_{i,j}\int_0^\beta \mathrm{d}\lambda\,\left\langle \mathrm{e}^{-\mathrm{i}\boldsymbol{Q}\cdot\widehat{\boldsymbol{r}}_i(0)}\mathrm{e}^{-\lambda\widehat{H}}\mathrm{e}^{\mathrm{i}\boldsymbol{Q}\cdot\widehat{\boldsymbol{r}}_j(t)}\mathrm{e}^{\lambda\widehat{H}}\right\rangle \quad (7)$$

where $\beta = 1/K_BT$ and the angular brackets denote a quantum statistical average. In the classical limit ($\beta \to 0$, $\hbar \to 0$) the operators $\widehat{A}$ become classical commuting dynamical variables and $K_q(Q,t) \to F_{cl}(Q,t)$. It can be shown [22] that $K_q(Q,t)$ is a real even function of time, so its spectrum $K_q(Q,\omega)$ is an even function of frequency. On the other hand, the experimental scattering cross section involves the Fourier transform $S_q(Q,\omega)$ of the quantum density correlator

$$F_q(Q,t) = (1/N)\sum_{i,j}\left\langle \mathrm{e}^{-\mathrm{i}\boldsymbol{Q}\cdot\widehat{\boldsymbol{r}}_i(0)}\mathrm{e}^{\mathrm{i}\boldsymbol{Q}\cdot\widehat{\boldsymbol{r}}_j(t)}\right\rangle.$$

The relation between $S_q(Q,\omega)$ and $K_q(Q,\omega)$ reads [22]

$$S_q(Q,\omega) = \frac{\beta\hbar\omega}{1-\mathrm{e}^{-\beta\hbar\omega}}K_q(Q,\omega)$$

and satisfies the detailed-balance condition. Moreover the condition

$$\Omega_K^{(2n)} = \frac{2}{\beta\hbar}\Omega_S^{(2n-1)} \quad (8)$$

relates the even frequency moments of K_q with the odd ones of S_q. The same memory function framework of equation (4) can be phrased for the Kubo relaxation function and for its Laplace transform $\widetilde{K}_q(Q,z)$.

By virtue of all these properties, in a situation where the quantum aspects not associated with detailed balance are marginal, it is reasonable (although not strictly rigorous) to identify the spectrum $K_q(Q,\omega)$ with the classical quantity $S_{cl}(Q,\omega)$ with the result that

$$S_q(Q,\omega) \simeq \frac{\beta\hbar\omega}{1-\mathrm{e}^{-\beta\hbar\omega}} S_{cl}(Q,\omega). \tag{9}$$

Having established such a correspondence, from now on we will drop the subscript *cl* and refer to the classical quantities as was in fact done at the beginning of this section.

2.2. The memory function features

The memory function $M(Q,t)$ accounts for all the relaxation mechanisms affecting collective dynamics, and consequently is the central quantity in most theoretical approaches. From straightforward algebra, the initial value of $M(Q,t)$ is related to the spectral moments of $S(Q,\omega)$ by

$$M(Q,t=0) = \frac{\Omega_S^{(4)}(Q)}{\Omega_S^{(2)}(Q)} - \Omega_S^{(2)}(Q). \tag{10}$$

An exact expression for $\Omega_S^{(4)}(Q)$ exists, but it involves the derivatives of both the interparticle potential and the pair distribution function [7]. It is usual to define $\omega_L^2(Q) = \Omega_S^{(4)}(Q)/\Omega_S^{(2)}(Q)$ and $\Delta^2(Q) = \omega_L^2(Q) - \omega_0^2(Q)$, their meaning being evident from the following argument. For sufficiently large $|z|$, $\widetilde{M}(Q,z) \simeq M(Q,t=0)/z$, and equation (6) is seen to have poles at

$$z = \pm\mathrm{i}\sqrt{\omega_0^2(Q) + \Delta^2(Q)} = \pm\mathrm{i}\omega_L(Q)$$

showing that the frequency $\omega_L(Q)$ characterizes the instantaneous collective response of the liquid at the wavevector Q. Similar remarks can be made for the generalized infinite-frequency velocity $c_\infty(Q) \equiv \omega_L(Q)/Q$.

In liquid systems, in the long-time limit, one expects $M(Q,t\to\infty)$ to approach the zero value; therefore, regardless of the details of its shape, $M(Q,t)$ it is expected to decay over a certain timescale $\tau(Q)$ that, for the sake of simplicity, can be defined as $\tau(Q) = \mathrm{M}(Q)/\Delta^2(Q)$, where

$$\mathrm{M}(Q) = \int_0^\infty M(Q,t)\,\mathrm{d}t.$$

It can be of considerable interest to investigate the asymptotic behaviours of equation (2) in the opposite regimes $\tau(Q)\omega_0(Q) \ll$ or $\gg 1$. In the first limit ($M(Q,t) \approx 2\mathrm{M}(Q)\delta(t)$) equation (2) reduces to the equation for a *damped harmonic oscillator*, and it can be easily proved that $M'(Q,\omega) = \mathrm{M}(Q)$ and $M''(Q,\omega) = 0$, which means two inelastic peaks in $S(Q,\omega)$ (in the current spectra they are centred at $\pm\omega_0(Q)$) damped with a factor $\mathrm{M}(Q)$. In the opposite limit, $\tau(Q)\omega_0(Q) \gg 1$, the characteristic decay time of $F(Q,t)$ is much higher than $\tau(Q)$, and $M(Q,t)$ appearing in the convolution integral of equation (2) can be considered constant, $M(Q,t) \approx \Delta^2(Q)$. Therefore equation (2) becomes non-homogeneous and the solution of equation (5) reduces to a *harmonic oscillator* of frequency $\omega_L(Q)$ with no damping, plus a *sharp elastic line*. In this extreme case, the intensity ratio of the elastic and inelastic lines (the Debye–Waller factor) in $S(Q,\omega)$ is $f(Q) = 1 - \omega_0^2(Q)/\omega_L^2(Q)$.

The true time dependence of the memory function is *a priori* unknown, and from the very start it is convenient to separate in $M(Q,t)$ the decay channels which explicitly involve couplings to thermal fluctuations ($M_{th}(Q,t)$) from those directly associated with longitudinal

density modes ($M_L(Q,t)$). A convenient way to perform this splitting is by the use of the generalized hydrodynamics theory [7,20]. In the simplest version of this approach, one writes

$$M(Q,t) = M_L(Q,t) + M_{th}(Q,t) = \Delta_L^2(Q)m_L(Q,t) + \Delta_{th}^2(Q)m_{th}(Q,t) \tag{11}$$

with

$$\Delta_L^2(Q) \equiv \omega_L^2(Q) - \gamma(Q)\omega_0^2(Q) \qquad \Delta_{th}^2(Q) = [\gamma(Q) - 1]\omega_0^2(Q).$$

Here $\gamma(Q)$ is a generalization of the specific heat ratio $\gamma = C_P/C_V$ to finite wavevectors. The relaxation processes underlying the dynamics are accounted for by the normalized quantities $m_L(Q,t)$ and $m_{th}(Q,t)$, defined in such a way that $m_L(Q,0) = m_{th}(Q,0) = 1$. A straightforward generalization of ordinary hydrodynamics suggests for the thermal contribution the following form:

$$m_{th}(Q,t) \approx \exp[-a(Q)Q^2 t] \tag{12}$$

where $a(Q)$ can be viewed as a finite-Q *generalization* of the quantity $D_T = \kappa/nC_v$, κ being the thermal conductivity. The role of the thermal contribution in the dynamic structure factor of liquid metals will be discussed in the following section.

In contrast with the case for the thermal decay channel, no guidance for $M_L(Q,t)$ is provided by ordinary hydrodynamics. In the latter case, one implicitly assumes that

$$M_L(Q \to 0, t) \approx 2(\eta_L/nm)Q^2\delta(t) \tag{13}$$

where the longitudinal viscosity coefficient η_L is related to the ordinary shear and bulk viscosities by $\eta_L = (4/3)\eta + \eta_B$. Clearly in the limit $Q \to 0$ the ratio $\widetilde{M}_L(Q, z=0)/Q^2$ approaches η_L/nm.

The simplest way to go beyond the hydrodynamic result (13) is to allow for a finite decay rate of $M_L(Q,t)$:

$$M_L(Q,t) = \Delta_L^2(Q)\mathrm{e}^{-t/\tau(Q)} \tag{14}$$

where we have additionally assumed an exponential lineshape for the memory function. Although this has the advantage of analytical simplicity when dealing with Fourier transform, a drawback of this *ansatz* lies in the violation of some basic short-time features of the memory function (such as a zero derivative at $t = 0$), causing the divergency of $\Omega_S^{(n)}$ for $n \geqslant 6$.

Equation (14) yields the so-called *viscoelastic model* for $S(Q,\omega)$ [22]. Since as $Q \to 0$, $\widetilde{m}_L(Q, z=0)/Q^2$ can written as $[c_\infty^2 - c_0^2]\tau(Q \to 0)$, the requirement that this coincides with η_L/nm shows that the time $\tau(Q)$ must be finite as $Q \to 0$. Such a connection with viscous effects justifies the physical interpretation of the rate $1/\tau(Q)$ as a parameter giving an overall account of all relaxation processes by means of which the longitudinal response of the liquid is affected by time-dependent disturbances. In particular, for slow perturbations developing over a timescale $t \gg \tau(Q)$, the system can adjust itself to attain local equilibrium and the usual viscous behaviour. In contrast, for disturbances fast enough that $t \ll \tau(Q)$, the liquid responds instantaneously, with a solid-like (elastic) behaviour. The crossover between these limiting situations (times $t \approx \tau(Q)$, or frequencies ω such that $\omega\tau(Q) \approx 1$) is ultimately responsible for the gradual changes often detected in the sound dispersion of several liquids at increasing wavevectors.

Similar considerations can be applied to the $M_{th}(Q,t)$ contribution which involves the timescale $\tau_{th} = D_T^{-1}(Q)Q^2$; in this case the 'elastic response' is achieved in the hydrodynamic regime: $\omega_0(Q \to 0)\tau(Q \to 0) \propto c_0/Q \to \infty$, while the 'viscous response' emerges at short wavelengths. The crossover between the two limits embodies the transition between the adiabatic and isothermal regimes, and reflects the actual possibility for density fluctuations to decay by the thermal channel: at high frequencies there is no time for such conversion, and

the fluctuations evolve without heat transfer (higher speed of sound, no attenuation) while in the low-frequency limit there is enough time for the system to equilibrate with the result that an isothermal dynamics takes place (lower speed of sound, damped excitation).

These qualitative considerations are supported by the evolution of the poles of $\widetilde{C}_L(Q,z)$ at increasing wavevectors. Equations (11), (12) and (14) in fact imply that

$$\widetilde{M}(Q,z) = \frac{\Delta_L^2(Q)}{z+1/\tau(Q)} + \frac{\Delta_{th}^2(Q)}{z+a(Q)Q^2}. \tag{15}$$

In the hydrodynamic regime ($Q \to 0$) both the inequalities $|z| \ll 1/\tau(0)$ and $|z| \gg a(Q)Q^2$ are satisfied, and the poles are approximately located at

$$z \approx \pm \mathrm{i}\sqrt{\omega_0^2(Q\to 0) + \Delta_{th}^2(Q\to 0)} = \pm \mathrm{i}c_s Q$$

where $c_s \equiv \sqrt{\gamma}\, c_0$ is the adiabatic velocity of sound. At larger wavevectors different situations may arise: the one of interest to us is $|z| \ll a(Q)Q^2$, which is readily seen to cause a shift of the imaginary part of the poles toward an isothermal behaviour, i.e. $\omega \simeq \pm\omega_0(Q)$. The last limiting case occurs whenever the frequency ω becomes distinctly larger than $[1/\tau(Q)]$, which eventually yields poles at $z = \pm\omega_L(Q)$, as already noticed. Although appealing, the simplicity of the viscoelastic model can be deceptive. First of all, the model itself provides no clue as to the physical origin of the decay mechanisms leading to the rate $1/\tau(Q)$. Secondly, even ignoring this aspect and treating $1/\tau(Q)$ as a fitting parameter, the practical results of the model are rather unsatisfactory (see figure 5 in the following). These drawbacks of the simple viscoelastic model have been theoretically predicted, and found to some degree for a number of liquids as a result of a detailed analysis of MD spectra [7, 23]. However, to our knowledge, no cutting-edge analysis exists in the case of experimental measurements of the coherent dynamic structure factor, probably because of the aforementioned limits of the neutron technique.

The obvious remedy is to modify the simple *ansatz* (14) by allowing a more sophisticated decay of $M_L(Q,t)$. We adopted the following two-exponential *ansatz*:

$$M_L(Q,t) = \Delta_L^2(Q)\left[(1-\alpha(Q))\mathrm{e}^{-\gamma_1(Q)t} + \alpha(Q)\mathrm{e}^{-\gamma_2(Q)t}\right] \tag{16}$$

where the rate $\gamma_1(Q)$ is chosen to be larger than $\gamma_2(Q)$, so that the dimensionless factor $\alpha(Q)$ measures the relative weight of the 'slow' decay channel. Besides being more flexible than the viscoelastic model, we shall see that the *ansatz* (16) has the much more important merit that the presence of two different timescales does in fact have a definite physical interpretation.

The previous *ansatz* was proposed phenomenologically several years ago and tested against the MD results on LJ fluids [24]; it is interesting to note that an expression analogous to equation (16) has been implicitly introduced in the viscoelastic analysis of Brillouin-light-scattering (BLS) spectra of glass-forming materials (see for example reference [25]). In fact, in the works cited, the general expression for $M_L(Q,t)$ for a two-time exponential decay is always expressed as

$$M_L(Q,t) = \Delta_\mu^2(Q)\mathrm{e}^{-t/\tau_\mu} + \Delta_\alpha^2(Q)\mathrm{e}^{-t/\tau_\alpha} \tag{17}$$

with explicit reference to the so-called α-relaxation (structural relaxation) process as responsible for the long-lasting tail, and to the microscopic μ-process as an additional, faster, relaxation dominant over a very short timescale. To be more precise, in the BLS spectral window the condition $\omega\tau_\mu \ll 1$ holds, so the approximation

$$M_L(Q,t) = 2\Delta_\mu^2(Q)\tau_\mu\delta(t) + \Delta_\alpha^2(Q)\mathrm{e}^{-t/\tau_\alpha}$$

is customarily adopted as a fitting model. However, we will show in this work that such an approximation is no longer tenable in the case of liquid lithium at the IXS frequencies.

The origin, at the atomic level, of this fast decay channel is still an open issue: one of the purposes of the present paper is to point out the features of such relaxation and to inspect its nature. The rapidly decaying portion of $M_L(Q,t)$ is customarily attributed to largely uncorrelated collisional events, similar to those occurring in a dilute fluid. In addition, at the high densities typical of the liquid state, non-negligible correlations among the collisions can be expected, rendering an interpretation just in terms of 'binary' collisions no longer valid. While the magnitude of the correlation effects is relatively small and their build-up slow, once established their decay is even slower, and for $t > 1/\gamma_1(Q) \equiv \tau_\mu$ this relaxation channel dominates the decay of $M_L(Q,t)$, which consequently may exhibit a small but long-lasting 'tail'. The *ansatz* (16) can incorporate most of this physics: on the basis of the latter, one may reasonably anticipate that $\alpha(Q) \ll 1$, and that the time $1/\gamma_2(Q) \equiv \tau_\alpha$ is distinctly longer than $1/\gamma_1(Q) \equiv \tau_\mu$. In this picture, the best-fit values of the viscoelastic rate $1/\tau(Q)$ clearly represent some sort of 'weighted average' of $\gamma_1(Q)$ and $\gamma_2(Q)$. Finally, we may argue that with increasing Q (i.e. over a shrinking length scale) the magnitude $\alpha(Q)$ of the correlation effects should decrease, and that at higher temperatures the value of $\alpha(Q)$ at a given wavevector should equally decrease. On a general basis, the requirement that

$$\lim_{Q\to 0} M_L(Q, z=0)/Q^2 \to \eta_L/nm$$

now takes the form

$$(c_\infty^2 - c_0^2)\left[\frac{(1-\alpha(Q\to 0))}{\gamma_1(Q\to 0)} + \frac{\alpha(Q\to 0)}{\gamma_2(Q\to 0)}\right] \to \eta_L/nm. \tag{18}$$

The refined model (16) yields a dynamic structure factor given by

$$S(Q,\omega) = \frac{S(Q)}{\pi}\,\mathrm{Re}\left\{\omega_0^2(Q)\Big/\left(\mathrm{i}\omega + \frac{\Delta_\mu^2(Q)}{\mathrm{i}\omega+\gamma_1(Q)} + \frac{\Delta_\alpha^2(Q)}{\mathrm{i}\omega+\gamma_2(Q)} + \frac{\Delta_{th}^2(Q)}{\mathrm{i}\omega + a(Q)Q^2}\right)\right\}^{-1}. \tag{19}$$

3. The experiments

In this work we report the determination by means of IXS of the dynamic structure factor of liquid lithium in the wavevector range from 1.4 to 110 nm^{-1}, corresponding to $Q/Q_m \approx 5\times 10^{-2}$–5. The scanned energy range has been settled at each Q in order to detect all the scattered signal up to the tails region, where it becomes comparable to the background.

The experiment has been performed at the very-high-energy-resolution beamline ID16-BL21 at the European Synchrotron Radiation Facility. A monochromatic beam of 10^9 photons s^{-1} is obtained from a cryogenically cooled Si(111) double crystal followed by a high-energy-resolution monochromator operating in back-scattering geometry at selectable Bragg reflections [26]. The scattered beam is collected by perfectly spherical silicon crystal analysers operating in back-scattering and Rowland-circle geometry at the same reflection order as the monochromator. They were obtained by gluing $\simeq$12 000 perfect crystals of $0.6\times 0.6\times 2\ \mathrm{mm}^3$ on a spherical blank [27]. The overall energy resolution was measured using a plexiglass scatterer at a Q-value corresponding to the maximum of its structure factor where the diffusion is dominated by the elastic contribution, and it turns out to have approximately a Lorentzian shape.

Different configurations have been adopted depending on the Q-range explored. Below Q_m (25 nm^{-1}) we used simultaneously five analysers mounted on a horizontally rotating arm and with a fixed offset of 1.5°. Either the Si(9 9 9) or Si(11 11 11) reflections, corresponding to energy resolutions of 3.0 meV and 1.5 meV (FWHM) respectively, have been selected. At

higher Q-values, where the spectra start to broaden, we used a vertical scattering geometry based on a single analyser housed on a rotating arm that can reach more than a 150° scattering angle. In this configuration we selected the Si (7 7 7) reflection with an overall energy resolution of 8.5 meV FWHM. The Q-resolution was $\simeq\pm 0.2$ nm^{-1} and $\simeq\pm 0.35$ nm^{-1} in the horizontal and vertical geometries respectively. The momentum transfer is related to the scattering angle by the relation $Q = 2k_0 \sin(\theta_s/2)$.

Energy scans have been done by varying the temperature of the monochromator with respect to that of the analyser crystals. The absolute energy calibration of successive scans is better than 1 meV. Each scan took about three hours, and each Q-point spectrum was obtained from the average of 2–8 scans depending on the Bragg-reflection order and on the Q-transfer. The data were normalized to the intensity of the incident beam. In the Q–E region of interest, empty-vacuum-chamber measurements gave either the flat electronic detector background of 0.6 counts min^{-1} or, in the angular region corresponding to $9 < Q < 13$ nm^{-1}, a small elastic line due to spurious reflection of the beam entering the analysers. These background signals were subtracted from the data before any other data treatment was carried out. The chamber Kapton windows (each 50 μm thick) gave no detectable contribution to the scattered flux.

The uncapped liquid-lithium container was made out of austenitic stainless steel in contact with a resistive heater, used to keep the liquid at constant temperature. We selected two different values: one slightly above the melting point, $T = 475$ K, and the second at $T = 600$ K; we have not been able to reach higher temperatures with our experimental set-up due to the lack of windows. The 20 mm long sample, kept together by surface tension, was maintained in a 10^{-6} bar vacuum. The lithium was loaded in an argon glove box.

As far as experimental aspects are concerned, the *energy transfer* E between the probe (x-rays) and the sample (excitations) has always been measured in meV. To make contact with the traditional notation adopted in computer simulations, we will refer from now on only to the frequency $\omega = 2\pi\nu = E/\hbar$ expressed in ps^{-1} (a numerical factor of $\approx$0.659 ps^{-1}/meV produces such a conversion).

The IXS spectra of liquid lithium below Q_m (horizontal geometry) are reported in figure 1 at the indicated Q-values. The low-Q data show the Brillouin triplet structure with the energy of the inelastic peaks increasing with Q up to a Q-value of 12 nm^{-1}. This value is close to $Q_m/2$, as deduced from the $S(Q)$ reported in figure 2. The dispersion up to $Q_m/2$ can therefore be interpreted as that of the longitudinal acoustic branch in a first Brillouin pseudo-zone. Furthermore, similarly to what is found in the second Brillouin zone (BZ) of a crystal, we observe that, also in liquid lithium, the energy of the acoustic modes decreases with increasing Q from $Q_m/2$ to Q_m. Increasing Q above Q_m, i.e. in the 'third' or higher BZs, the spectrum increasingly broadens and distinct peaks are no longer observable. At the highest Q-values one finds that the dynamic structure factor becomes a symmetric peak centred at frequencies larger than $\omega = 0$, the behaviour expected for a quantum free particle (in the classical limit no recoil energy is expected). Such evolution can be clearly followed in figure 3. Beside the observation of dispersion in the first and second pseudo-BZs, it is also important to note that the broadening of the excitations increases monotonically with Q, to the extent that near the end of the second pseudo-BZ a well-defined inelastic peak is no longer visible.

In order to extract quantitative information from the experimental intensity, i.e. to perform measurements of $S_q(Q, \omega)$ on an absolute scale, the most direct method would be to use a reference scatterer as is customarily done in neutron experiments. In IXS studies such a procedure is extremely difficult because of the Q-dependence of the form factor and, in our case, the different efficiencies of the analysers. For these reasons we preferred to use an alternative indirect method based on the knowledge of the sum rules of $S_q(Q, \omega)$: in particular,

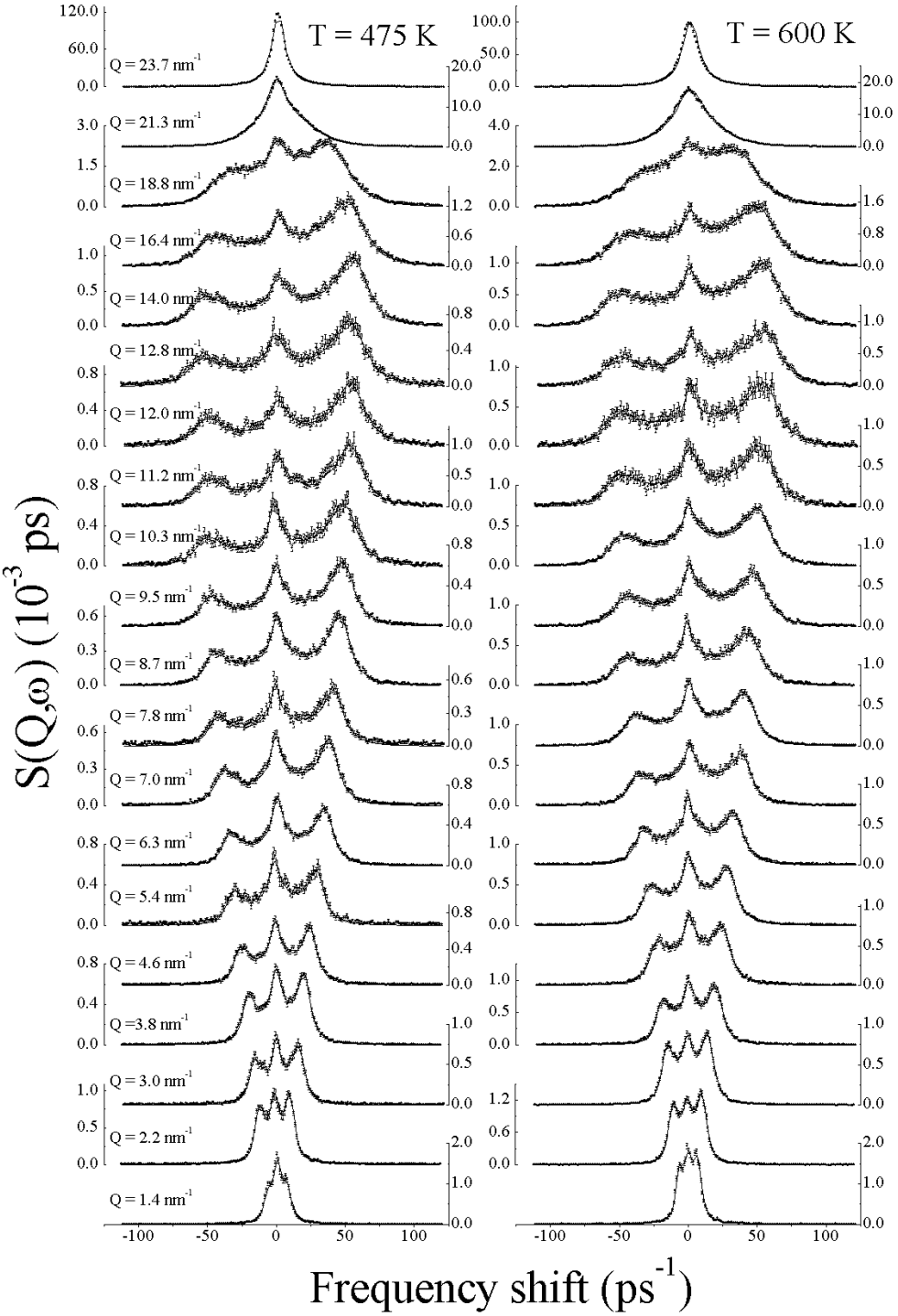

Figure 1. IXS spectra at selected values of $Q < Q_m$, in the (9 9 9) configuration, at two different temperatures. Each full line is a best fit taking into account thermal, slow and fast relaxations.

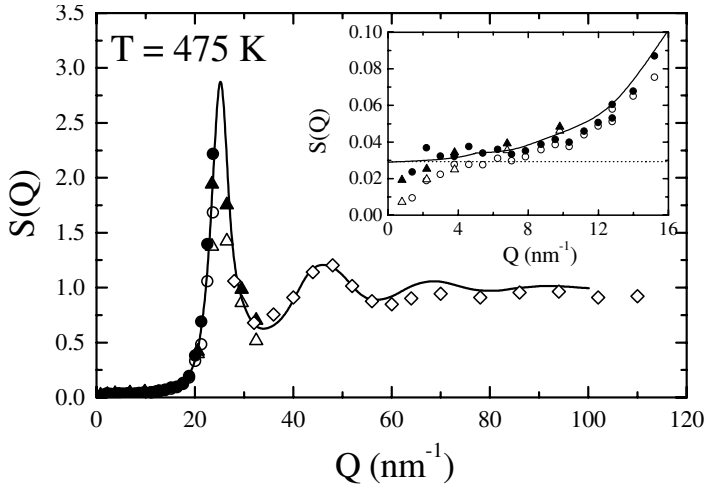

Figure 2. Comparison between the $S(Q)$ experimentally determined as discussed in the text and through the MD simulations (——) of reference [28]. Triangles (△): (11 11 11) data; dots (○): (9 9 9) data; lozenges (◇): (7 7 7) data. The full symbols are the values corrected for asymmetric resolution effects; at the higher Q-values such correction is negligible and is not reported. The inset shows on an enlarged scale the low-Q region.

for the first two frequency moments we have

$$\Omega_S^{(0)} = \int S_q(Q,\omega)\,\mathrm{d}\omega = S(Q)$$

$$\Omega_S^{(1)} = \int \omega S_q(Q,\omega)\,\mathrm{d}\omega = \hbar Q^2/2m$$

where the second equality follows from equation (8) applied for $n = 1$. The measured raw intensity is related to the dynamic structure factor through

$$I(Q,\omega) = A(Q)\int \mathrm{d}\omega'\, S_q(Q,\omega')R(\omega-\omega') \tag{20}$$

where $R(\omega)$ is the experimental resolution function and $A(Q)$ is a factor taking into account the scattering geometries, the experimental set-up and the lithium atomic form factor. The first moments of the experimental data, $\Omega_I^{(0)}$ and $\Omega_I^{(1)}$, and those of the resolution function, $\Omega_R^{(0)}$ and $\Omega_R^{(1)}$, are related to $\Omega_S^{(0)}$ and $\Omega_S^{(1)}$ by

$$\Omega_I^{(0)} = A(Q)\Omega_S^{(0)}\Omega_R^{(0)}$$

$$\Omega_I^{(1)} = A(Q)(\Omega_S^{(0)}\Omega_R^{(1)} + \Omega_S^{(1)}\Omega_R^{(0)}).$$

From the previous equation one derives that

$$S_q(Q) = \frac{\hbar Q^2}{2M}(\Omega_I^{(1)}/\Omega_I^{(0)} - \Omega_R^{(1)}/\Omega_R^{(0)})^{-1}. \tag{21}$$

This procedure has been adopted to establish an absolute scale for $S_q(Q,\omega)$ using the experimentally determined $I(Q,\omega)$ and $R(\omega)$. Its reliability is shown in figure 2 where we obtain an excellent agreement between the values of $S_q(Q)$ obtained from equation (21) and those derived from a MD simulation at $T = 475$ K [28]†. The reported MD data are the

† In this respect it is worth pointing out that as $S(Q)$ was calculated within the classical approximation (MD), it may in principle be different from the real one (IXS). In fact, it has already been shown that an excellent agreement exists between MD and INS experiments [12], so such a comparison is fully justified.

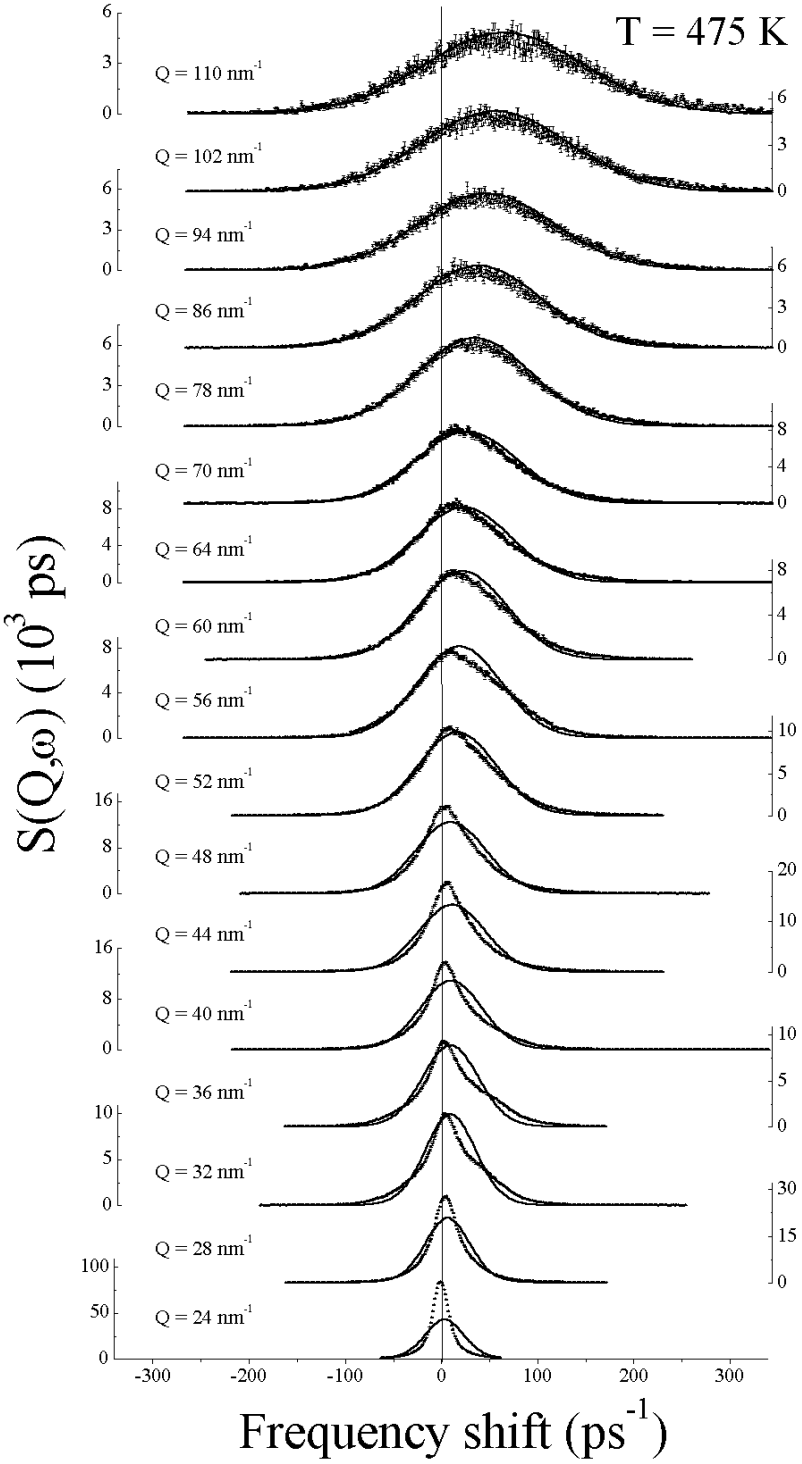

Figure 3. IXS spectra at Q-values above the main peak of the structure factor, in the (7 7 7) configuration, at the lower temperature. In each case, the full line is the theoretical lineshape expected in the single-particle, high-Q, limit.

outcome of a simulation carried out using the Price–Tosi interaction pseudopotential already tested against neutron diffraction data (see reference [12] for further details).

4. Data analysis

Lithium has been chosen because, among the simple monatomic liquids, is the one that is best suited to IXS investigation. Indeed, its low mass gives recoil energies observable in the Q-range considered, and its low atomic number and large velocity of sound give the optimal signal within the available energy resolution, compensating for the large form factor decrease at high Q-values. The $I(Q, \omega)$ spectra, reported at their absolute scale, exploiting the zeroth- and first-moment sum rules, show the transition from a triplet to a Gaussian. The maxima, $\omega_m(Q)$, of the longitudinal current spectra ($\omega^2 S(Q, \omega)/Q^2$) show an almost linear dispersion relation at low Q—typical of a sound wave—and a completely different dependence in the high-Q limit, where they approach the parabolic dispersion of the quantum free particle. Between these two regions, $\omega_m(Q)$ exhibits oscillations which are in phase with the structural correlations as observed in $S(Q)$.

The low-Q region is of particular interest for its large content of information. The so-called positive dispersion, a fingerprint of the relaxation dynamics of disordered systems, either liquid [1,2,6,12,13] or glassy [29,30], reflects the host of mechanisms driving such dynamics, their timescale and, on careful inspection, their nature. We will start our analysis from here.

4.1. The 'low-Q' region

Looking at the spectra in figures 1, 3, as also confirmed by the results reported in this section, the memory function approach can profitably be used approximately up to Q_m. We adopted the following procedure. The classical result of equation (5) was modified according to equation (9) to take into account the detailed-balance effects. The resulting $S_q(Q, \omega)$ was then convoluted with the instrumental resolution according to (20). The χ^2-function arising from the difference between the resulting function and the experimental data was finally minimized by a standard Levenberg–Marquardt routine. Among the fitting parameters, $S(Q)$ and $\omega_0^2(Q)$ are independent of the specific model for the memory function, and their value is basically known: the first has been calculated from the first-moment sum rule as discussed in section 3 (we have already discussed the approximation $S_q(Q) \cong S(Q)$), so it has been kept fixed during the iterations. Then the second quantity $\omega_0^2(Q)$ is simply deduced from its definition (see equation (3)). It is worth pointing out that $\omega_0^2(Q)$ *cannot be taken as the second-frequency moment of* $I(Q, \omega)$ for two main reasons. The first one, related to the effects of the resolution, may be in principle overcome by a procedure similar to the one leading to the determination of $S(Q)$, but with the further difficulties arising from the almost-Lorentzian shape of the resolution that leads to a diverging $\Omega_R^{(2)}$. Most severe is the *non-invariance of the second moment under the transformation* (9). For the sake of clarity we report in figure 4 the theoretical value $\omega_0^2(Q)$ compared to the second normalized moment of the experimental $I(Q, \omega)$ at $T = 475$ K: the latter is always larger (this may be due also to the small but non-vanishing background in the experimental data) and the agreement deteriorates with decreasing wavevector, as the resolution effects become dominant.

All the other fitting parameters obviously depend on the specific model for $M(Q, t)$. Let us firstly examine the spectral relevance for liquid Li of the coupling to thermal fluctuations, accounted for by the contribution $M_{th}(Q, t)$ to the total memory function. At not too high temperatures in the molten phase, all liquid alkali metals are characterized by a specific heat ratio $\gamma \approx 1$, the typical values giving $\gamma - 1 \simeq 0.1$. Outside the hydrodynamic ($Q \to 0$) regime

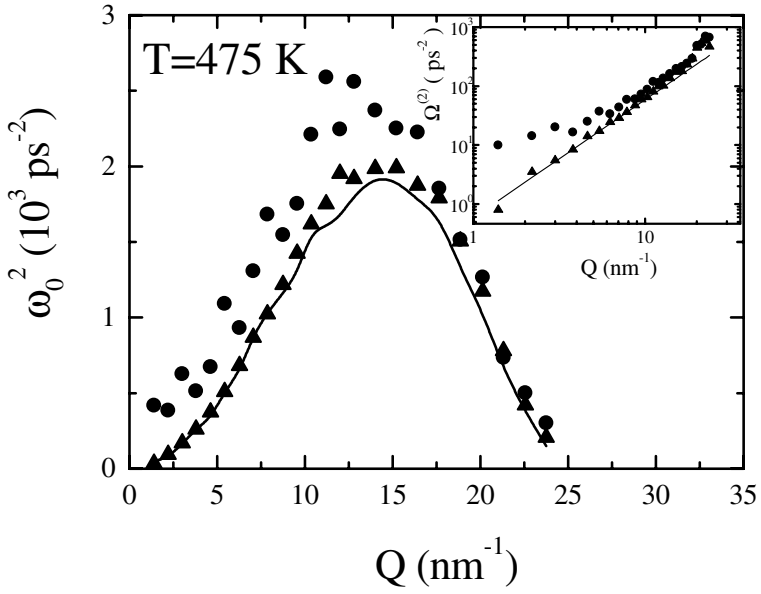

Figure 4. Comparison between the value of $\omega_0^2(Q)$ as calculated from its definition (——) and from the three-time fit (▲) leaving it as a free parameter. The normalized second-frequency moment of $I(Q, \omega)$ is also reported (•) to emphasize resolution and quantum effects. In the inset we show the same quantities non-normalized.

(and, in particular, in the wavevector range probed in this work) there are several indications that the difference $\gamma(Q) - 1$ is even smaller [13]†. Despite its modest strength in the present Q-range, the role of thermal relaxation in liquid metals is strikingly different from the one played for ordinary non-conducting liquids. A simple estimate of the decay rate embodied in $M_{th}(Q, t)$ reported in equation (12) based on the experimental values of the thermal conductivity and of the specific heat [31] shows that, for liquid lithium, $\omega \ll (\kappa/nC_V)Q^2$ for most of the spectral range of interest here, and in particular for the range characterized by the presence of inelastic peaks (see figure 1). This indicates that in liquid Li (but a similar argument is expected to hold in general for molten metals) the aforementioned transition from the adiabatic to the isothermal response occurs at wavevectors well *below* those probed in the present experiments. Indeed, for wavevector-independent thermal parameters (a reasonable assumption at so low a Q) we find for the threshold wavevector $\omega_0(Q^*)\tau_{th}(Q^*) = 1$ a value of $Q^* \simeq 0.2\,\mathrm{nm}^{-1}$ at $T = 475$ K, varying only by a few per cent from that at $T = 600$ K. Of course, this does not mean that the presence of thermal fluctuations has no influence: as shown for example by equation (15), and as can be inferred by the simple arguments of section 2.1, they may still give some contribution to the real part of the memory function, i.e. ultimately to the Brillouin-peak widths. Such a linewidth contribution gives $\delta\omega_{th} = \Delta_{th}^2\tau_{th} = (\gamma(Q) - 1)c_0(Q)/D_T(Q) \cong 0.056$ ps^{-1} (0.07 ps^{-1}) for $T = 475$ K ($T = 600$ K) (in the $Q \to 0$ limit) and is not explicitly dependent

† Here, reference is made to the molecular dynamics computations of Canales *et al* [13]. For liquid Li at 470 K, these authors report a monotonic decrease of the value of $\gamma(Q)$ from 1.11 at $Q = 2.55$ nm^{-1} down to 1.01 at $Q = 18.4$ nm^{-1}. This trend changes only when Q approaches the position $Q_m \simeq 25$ nm^{-1} of the main peak of the static structure factor: here there is a sudden increase of $\gamma(Q)$ to values $\simeq$1.4. Ultimately, one expects that at even larger wavevectors, $\gamma(Q)$ should approach the limiting value $5/3 \simeq 1.67$ appropriate for a non-interacting monatomic system. Needless to say, any recourse to generalized hydrodynamics arguments becomes increasingly doubtful for wavevectors distinctly larger than Q_m.

on Q. As already remarked, such a contribution may be of some relevance only at the first two or three Q-values investigated here, but *the strongly Q-dependent broadening of the inelastic components has to be ascribed to some other dynamical process*. On the basis of the same argument, it is worth pointing out that *the hydrodynamic value of the speed of sound is not yet reached at the lower Q-values of this work*: as far as the positive dispersion is concerned, in the present case, *the lower edge of the transition is the isothermal rather than the adiabatic value*. As previously noted, a completely different scenario characterizes non-metallic fluids: due to the much lower thermal diffusivity, the opposite thermal regime is experienced throughout the collective excitation region and the final low-Q result is an adiabatic response without any damping of the sound waves and with a narrow elastic line.

Having ascertained the role of thermal effects, we now come to the more important implications of the fitting analysis for the dynamics of $m_L(Q,t)$. In the following we will refer to figure 5 where the specific situation of the spectrum at $Q = 7\ \mathrm{nm}^{-1}$ has been chosen to clarify the lineshape details associated with the different contributions to the memory function.

As a zero-level approximation we consider the lineshape obtained from the simple hydrodynamic expression which only accounts for thermal decay processes, taking all the other relaxation channels as instantaneous: beside the use of equations (11), (12), this is simply done assuming that $m_L(Q,t) \propto \delta(t)$. As in our case even the thermal relaxation is quite rapid on the x-ray timescale, the net result is a lineshape close to that of the damped harmonic oscillator model. It is therefore not surprising (see figure 5) that the agreement with experimental data is very poor (no elastic peak is reproduced). Consequently, the assumption of an instantaneous decay of $m_L(Q,t)$ is untenable.

Following section 2.2, as a next step, we generalize the memory function using expression (15), i.e. the viscoelastic model. All the merits and the drawbacks of this model are again illustrated in figure 5. Leaving the time $\tau(Q)$ and the strength $\Delta_L^2(Q)$ as fitting parameters, it is possible to obtain a rather good agreement for the position of the inelastic peaks, and consequently for the main features of the dispersion of sound-like excitations. However, one notes clear discrepancies in the quasi-elastic region at small ω. The fitting procedure yields, with comparable χ^2-values, two different sets of parameters, corresponding to two different timescales driving the dynamics of the system. More precisely, in one case the broader parts of the quasi-elastic and the Brillouin lineshapes are well reproduced but the narrow quasi-elastic part is missing, while in the other case the narrow elastic peak is well fitted but the Brillouin lines are too sharp. In other words, *the viscoelastic model cannot account for the double-sloped shape of the quasi-elastic region*. Although in figure 5 we refer to $Q = 7\ \mathrm{nm}^{-1}$, the situation at most wavevectors is similar.

The inescapable conclusion is that there are at least two different timescales, each giving a contribution to the width of the 'quasi-elastic' region, and accounting at the same time for the inelastic lineshape. On these grounds, the more flexible phenomenological model (16), based on two exponential decays, appears more promising. In this case the best-fitted lineshapes (quantum corrected and resolution convoluted), including the thermal relaxation (using the values for $Q \to 0$ of the specific heat ratio and thermal diffusivity from [31]) through equation (19), are again reported in figures 1 and 5, and a marked improvement of the agreement is clearly visible.

In figure 6 we also report the classical and resolution-deconvoluted lineshapes of $S(Q,\omega)$ and $C_L(Q,\omega)$ as built from the fitting parameters, in the region $Q < 14\ \mathrm{nm}^{-1}$, the most significant as far as the positive-dispersion task is concerned. The maxima of the latter function have been utilized to determine the apparent velocity of sound for the system.

Let us now discuss the different parameters entering equation (16), starting from the relaxation times: in figure 7 we report the wavevector dependence of such quantities at both

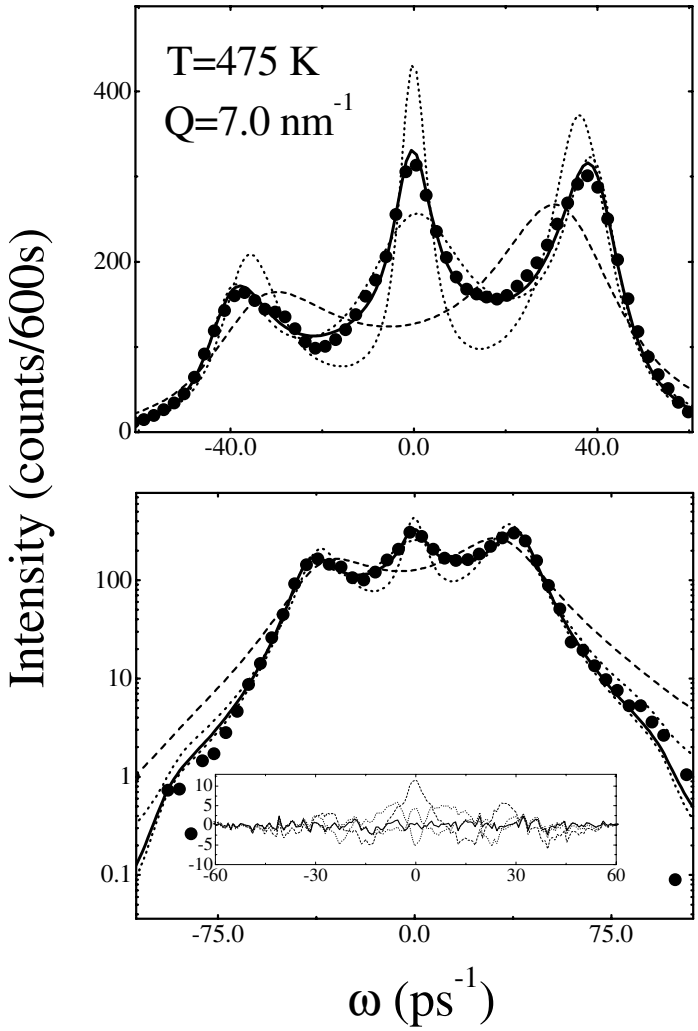

Figure 5. Inelastic x-ray scattering spectra of lithium at $T = 475$ K and $Q = 7.1$ nm^{-1}. Dots (•): experimental data; dashed line (– – –): the simple hydrodynamic fit (DHO); dotted lines (· · · · · ·): the simple viscoelastic model (thermal and one relaxation time) showing two different scenarios of comparable χ^2; full line (——): thermal and two relaxation times, structural and microscopic. The inset shows the mean square deviations for the different models.

temperatures. The presence of the double timescale is confirmed by the difference by about one order of magnitude between the two parameters τ_α and τ_μ. As regards τ_α it is worth pointing out the non-negligible effect of resolution: the value of 1/HWHM is comparable to the relaxation time itself, so it is expected to affect this fitting parameter, particularly at low Q. As a consequence it is unfortunately not possible to inspect any temperature dependence of $\tau_\alpha(Q, T)$. Completely different is the situation as far as the fast timescale is concerned. The determination of τ_μ is expected to be definitely more reliable and on the basis of our analysis the fast dynamics turns out to be temperature independent at the Q-values investigated. The influence of these relaxation mechanisms on the dynamics can be inferred looking at the values of $\omega(Q)\tau(Q)$, as was done before for the thermal channel: as far as the slow mechanism is

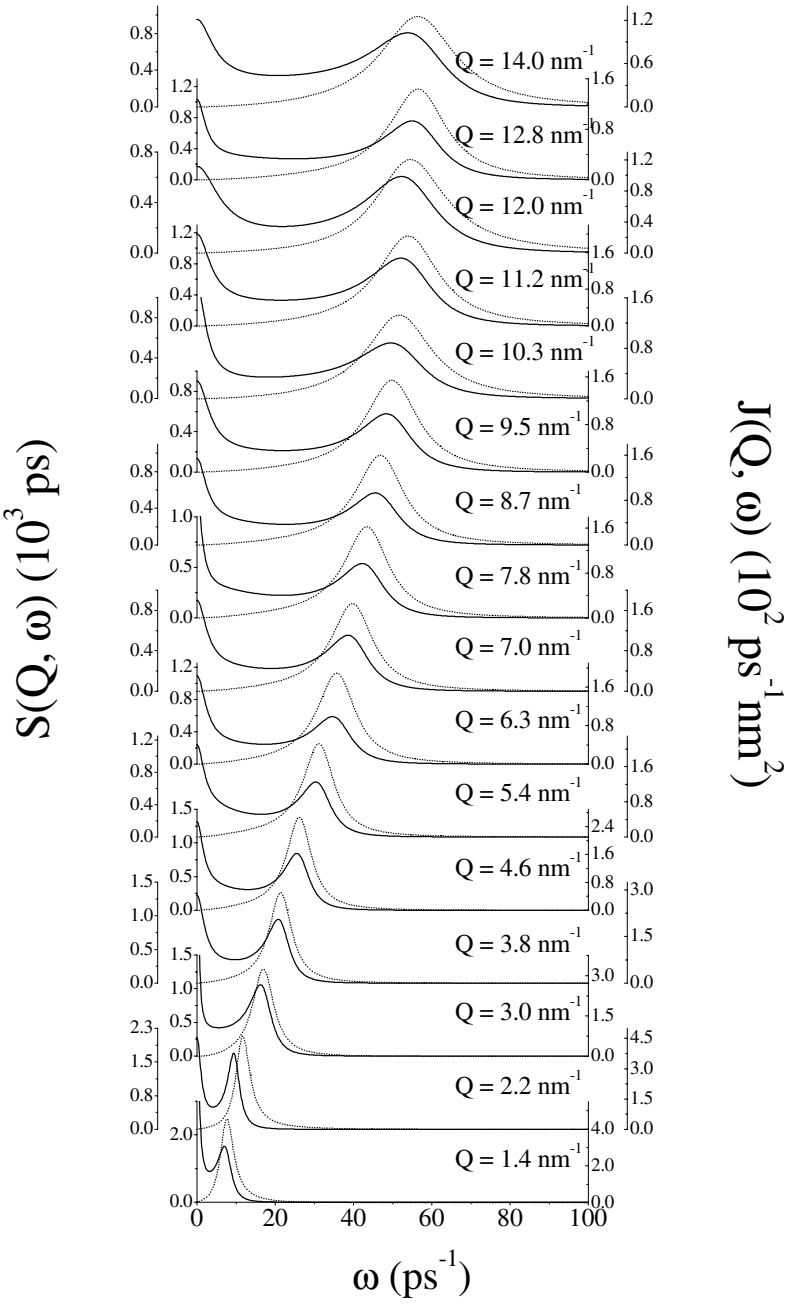

Figure 6. The dynamical structure factor $S(q, \omega)$ (——) and longitudinal current correlation function $C_L(Q, \omega)$ (· · · · · ·) in the low-Q region as obtained from the two-time fitting model (classical and resolution deconvoluted). The (symmetrical) peak positions of the latter quantity have been utilized to determine the apparent speed of sound of the system.

concerned the system response turns out to be 'solid-like' across the full first Brillouin pseudo-zone (see the insets in figure 7(a)). The fast relaxation accounts instead for a moderately viscous

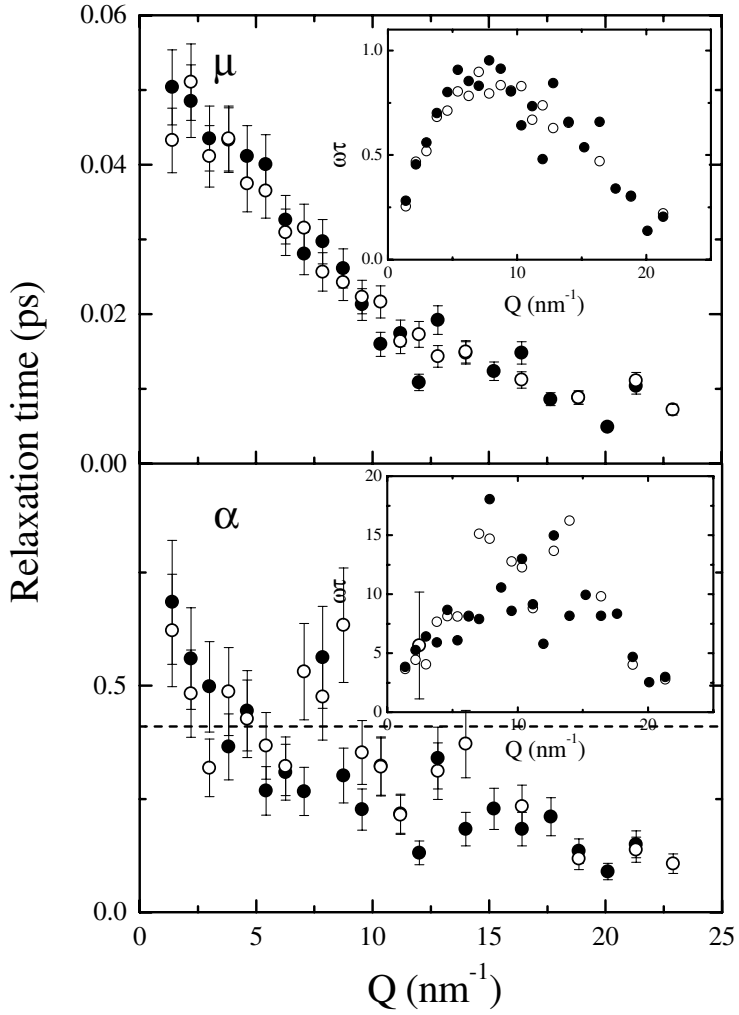

Figure 7. Relaxation times at different temperatures from the fits. Full symbols: $T = 475$ K; open symbols: $T = 600$ K. The timescale corresponding to the experimental resolution (3.0 meV) is also reported (− − −) to show how it could affect the lower-relaxation-time determination.

response: $\omega(Q)\tau(Q) \sim 1$ around the peak value at $Q \simeq 8$ nm^{-1} and remains quite low all around (see the insets in figure 7(b)). Following the arguments of section 2.2, we expect the slow relaxation to be responsible for the narrow quasi-elastic contribution and for the position of the inelastic features of $S(Q, \omega)$ while the fast process should be the main driver of the acoustic damping (Brillouin linewidth), also accounting for the broader part of the Mountain peak [32].

To go further and identify the real quantitative influence of such two channels, it is necessary to look at the strength parameters, or better at the rate $\alpha(Q)$. Such a quantity, defined as the ratio $\Delta_\alpha^2/(\Delta_\mu^2 + \Delta_\alpha^2)$, has its maximum of $\simeq$0.20 at low Q and decreases with increasing wavevector as shown in figure 8. This means that the fastest process plays the major role in characterizing the dynamics of liquid throughout the investigated first Brillouin pseudo-zone. Such a statement can be better understood by looking at the apparent speed-of-sound behaviour

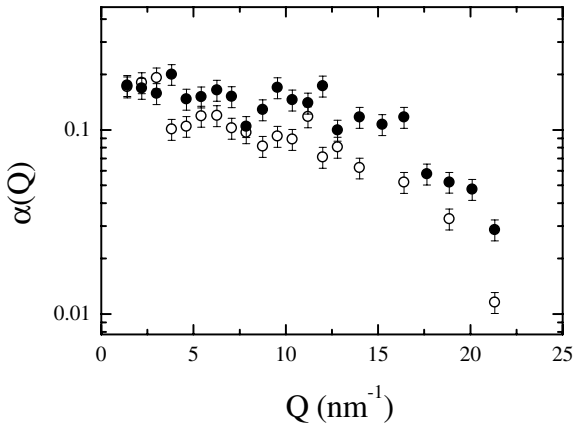

Figure 8. The ratio between the slow and the total relaxation strength. Full dots (•): $T = 475$ K; open dots (○): $T = 600$ K.

as plotted in figure 9. The velocity of sound moves from the low-Q value (isothermal in the IXS window) to its high-frequency value $c_\infty(Q)$. As previously noted, such behaviour has been observed in several MD simulations of alkali metals and in some cases experimentally, even if with some ambiguity due to kinematic restrictions/incoherent contributions on the neutron side and resolution broadening in the pioneer IXS experiments [14]. What is less clear is the microscopic origin of such a positive dispersion. On the basis of our analysis, once we have

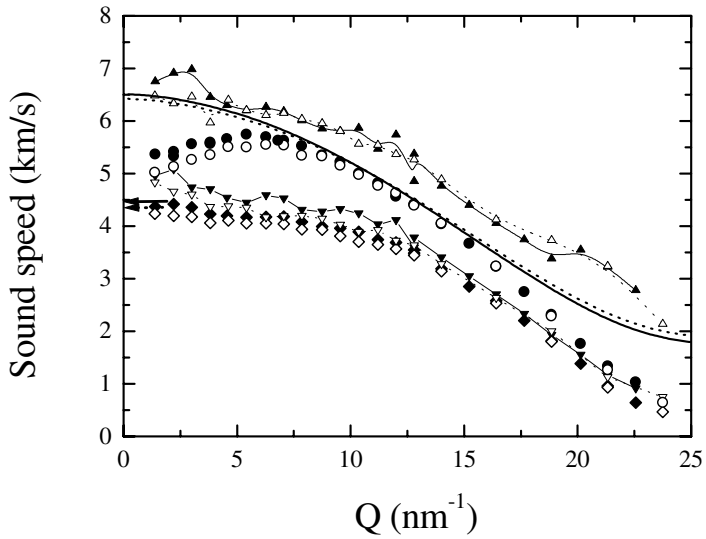

Figure 9. The apparent speed of sound (○), from the maxima of $J(Q, \omega)$ built from the fit parameters (and therefore resolution deconvoluted), compared to the hydrodynamic limit of reference [31] (←– – arrow on the left) and to the high-frequency limit $c_\infty^{th}(Q)$ (· · · · · ·) of reference [28]. The following quantities, deduced from fitting parameters, are also reported: the isothermal speed of sound $c_0(Q)$ (◇), the high-frequency limit associated with the slow process $\sqrt{\{\omega_0^2(Q) + \Delta_\alpha^2(Q)\}}Q$ (−▽−) and finally the total $c_\infty(Q)$ (− △ −) with all the strengths included. The full lines/symbols denote $T = 475$ K data; the dotted lines/full symbols relate to $T = 600$ K.

unambiguously found experimental evidence of a double timescale, *we are able to ascribe the positive dispersion of the velocity of sound to the faster process*. We reported in fact in figure 9 the value of the solid-like response associated with the single slow process and with both slow and fast relaxation processes. As expected, the 'jump' in the velocity of sound associated with the slow α-process, namely $[\sqrt{\{\omega_0^2(Q) + \Delta_\alpha^2(Q)\}} - \omega_0(Q)]/Q$, has already occurred at the lower IXS Q-values, but it is quantitatively negligible as compared to the full positive dispersion of the system. Despite the fact that the condition $\omega_l(Q)\tau_\mu(Q) \gg 1$ is never satisfied, *the faster process, due to its dominant strength, accounts almost entirely for the viscous–elastic transition*. As can be seen in figure 9, the apparent velocity of sound $c_{app} = \omega_l(Q)/Q$, never reaches the infinite-frequency velocity of sound deduced from the fit:

$$c_\infty(Q) = \sqrt{\omega_0^2(Q) + \Delta_\alpha^2(Q) + \Delta_\mu^2(Q)}\big/Q.$$

At first sight this discrepancy may seem to be explained by the fact that $\omega_l(Q)\tau_\mu(Q)$ is always $\sim$1. However, $c_\infty(Q)$ can also be evaluated theoretically starting from the knowledge of the interatomic potential and the pair distribution function (see for example reference [7]). In figure 9 we also report the values [28] of the unrelaxed speed of sound $c_\infty^{th}(Q)$ computed in this way; they turn out to be lower than those determined from the fitting of the spectra at both the temperatures. Moreover, $c_\infty^{th}(Q)$ is actually reached by the apparent speed of sound at $Q \cong 9$ nm^{-1}, i.e. when $\omega_l(Q)\tau_\mu(Q) \sim 1$.

A possible explanation of the inconsistency between $c_\infty^{th}(Q)$ and $c_\infty(Q)$ defined above is related to the arbitrary choice of the memory function details. Even though the presence of a two-timescale dynamics is directly seen in the raw experimental data (particularly in the $7 < Q < 14$ nm^{-1} region; the quasi-elastic peak reflects the superposition of two peaks of different widths), the detailed shape of $M_L(Q, t)$ can have in principle more complicated features than the double-exponential *ansatz* of equation (16). In particular we already mentioned the major drawback of such an assumption, namely the cusp at $t = 0$. It is reasonable to think that an exponential decay forced to represent a more complicated time dependence can give an accurate estimate as far as τ is concerned, while at short times the lack of a zero second derivative inescapably leads to an overestimate of $M_L(Q, t = 0)$, i.e. just the positive-dispersion amplitude; a similar effect, i.e. the overestimation of $c_\infty(Q \to 0)$ deduced from the fit of BLS data using instantaneous approximation for the microscopic process with respect to the maxima of the experimental IXS current spectra, has been recently shown for polybutadiene [33].

The last important aspect concerns the relative weights of the two processes and how to relate them to the acoustic attenuation. The role of the thermal effects has already been discussed. Looking at the generalized viscosity contributions $\Delta_\mu^2\tau_\mu$ and $\Delta_\alpha^2\tau_\alpha$ (see figure 10) we find that they are nearly comparable (the strength differences are nearly balanced by the different τ), but once again only the microscopic (faster) relaxation process can be related to the Brillouin linewidth, being the only one close to the $\omega\tau \ll 1$ condition in the Q-range explored. Moreover, in the spirit of the hydrodynamic generalization, the sum of such contributions is expected to have a Q^2-dependence. Such a prediction is quite well reproduced by our fits: only at very low Q does a slight deviation occur, ascribable to the slow part; once again the reason may be an excessive estimate of the α-relaxation time at small Q. Finally, in figure 11, the longitudinal viscosity as the outcome of the fit (the full area under $M(Q, t)$) is compared to an experimental determination of shear static ($Q \to 0$) viscosity [31]. Noting that for molten alkali metals the shear part usually accounts for 30–40% of the longitudinal part, the agreement is satisfactory, except at the points at very low Q, where finite-resolution-function effects prevent an accurate check.

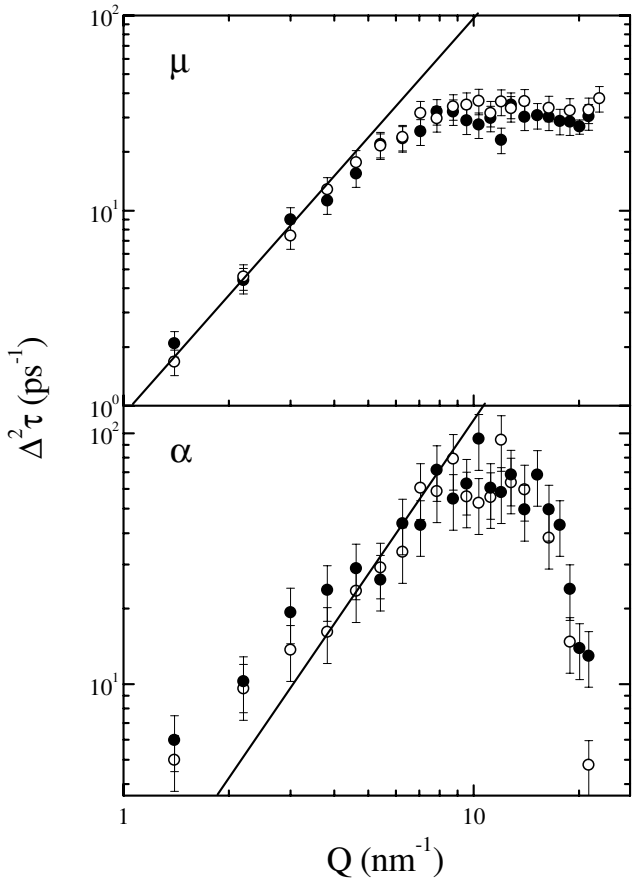

Figure 10. The viscosity contribution $\Delta^2\tau$ of the fast and slow relaxation; full dots (•): $T = 475$ K; open dots (○): $T = 600$ K. The Q^2-dependence is also shown for comparison (full line (——)).

4.2. The 'high-Q' region

Above Q_m, collective excitations are still evident in $I(Q, \omega)$ for nearly one more Brillouin pseudo-zone, even if the analysis of the previous section is not wholly satisfactory because of the worsening of the experimental resolution. Moreover, single-particle features gradually emerge, giving rise to a crossover between two completely different dynamical regimes. As the density-fluctuation wavelength matches the mean interparticle distance, a transition between strongly correlated and incoherent motion occurs. The lineshape associated with a quantum free particle is well known to be Gaussian. Once $S_q(Q)$ is determined as before from the sum rules for the first two moments, there are no unknown parameters. While in the previous section our sample has been supposed to be a single-component one, we must now, due to the emergence of an additional quantum effect, enhance the accuracy by taking into account isotopic effects. From the natural abundance ratios (92% of ^{7}Li, 8% of ^{6}Li) one finds that

$$S_q(Q, \omega) = \frac{1}{\sqrt{2\pi}} \sum_{i=6,7} \frac{C_i}{\sigma_i} \mathrm{e}^{-(\omega-\omega_i)^2/2\sigma_i^2} \tag{22}$$

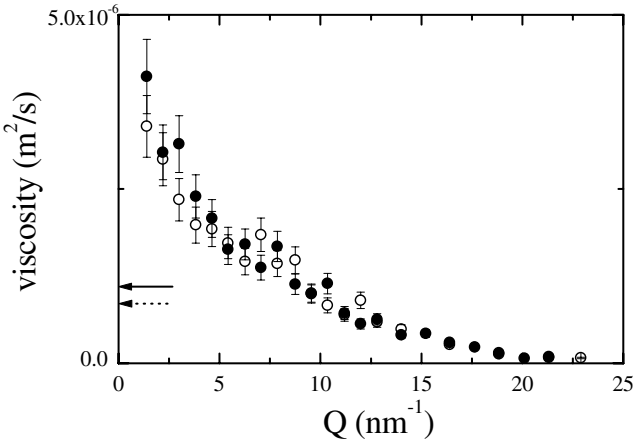

Figure 11. The longitudinal viscosity from the fit $(\Delta_\alpha^2\tau_\alpha + \Delta_\mu^2\tau_\mu)/Q^2$ compared to the shear viscosity data of reference [31]. The full lines/symbols denote $T = 475$ K data; the dotted lines/open symbols relate to $T = 600$ K.

where the C_i are the above-mentioned isotope concentrations while $\omega_i = \hbar Q^2/2m_i$ and $\sigma_i^2 = K_B T Q^2/m_i$ are the first (central) and the second (relative to ω_i) frequency moments of the two isotopes. In figure 3 the experimental spectra are reported together with the theoretical lineshapes (resolution convoluted) of equation (22) in order to emphasize all the crossover features. To be more quantitative we report in figure 12 the Stokes-current spectra maxima ω_l as a function of the exchange wavevector. Indeed, in this 'high-Q' region (above $Q_m = 24\,\mathrm{nm}^{-1}$) this quantity has been calculated starting from the spectra of figure 3 (we expect the effect of

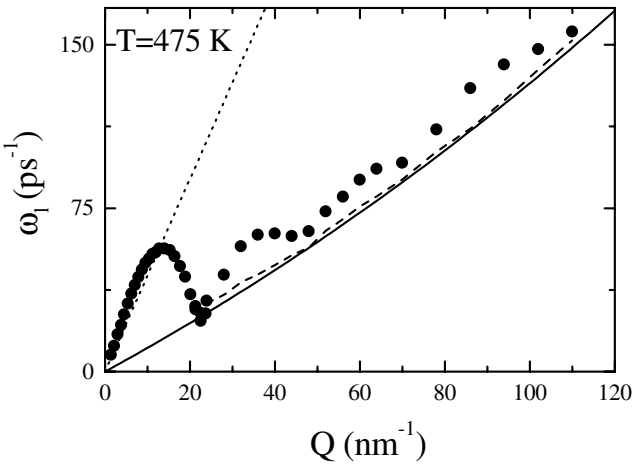

Figure 12. Maxima of the current spectra (•) for the full range of wavevectors explored at $T = 475$ K, compared to the asymptotic opposite behaviours in the limits of low Q (hydrodynamic (· · · · · ·); from reference [31]) and high Q (quantum free particle (——); see the text). As far as (7 7 7) data are concerned, we reported the rough current maxima as calculated from the spectra. To estimate the resolution effect, we also include in this case the high-Q-limit value as deduced from the free-particle model folded with the instrumental resolution.

the resolution broadening to be negligible at such high Q-values). For this reason, due to the quantum features of $S(Q, \omega)$, the quantity ω_l takes different values on the Stokes/anti-Stokes sides of the spectra†. The asymptotic values are expected to be reached in the regions of very low Q (adiabatic) and high Q (free particle)‡.

After an initial nearly linear dispersion, structural effects take place suppressing the propagation of sound around $Q_m/2$ due to strong negative interference. With increasing Q-value, the points in figure 12 show not only a second pseudo-BZ, but also a series of oscillations that damp out with increasing Q—here, $\omega_l(Q)$ is approaching the single-particle behaviour. These oscillations are in anti-phase with those of $S(Q)$ (see figure 2) and can therefore be associated with the local order in the liquid.

5. Conclusions

In the present work inelastic x-ray scattering has been utilized to study in detail the main features of the collective dynamics in liquid lithium, a system for which the use of inelastic neutron scattering is quite difficult and basically impossible in the low-Q region. These IXS experiments have allowed a precise assessment of the different relaxation processes which affect the spectral shape of the dynamic structure factor. Specifically, the quality of the data required an analysis where one has to invoke the simultaneous presence of three distinct decay channels of the collective memory function. The first one is associated with the coupling between density and temperature fluctuations. As for other alkali metals, although its relevance is rather small, this process cannot be neglected and plays a different role to that for ordinary non-conducting liquids. Much more important is the unambiguous evidence of *two well-separated timescales* in the decay of $M_L(Q, t)$—the portion of the memory function directly associated with generalized viscosity effects. In this respect, our IXS data prove that the traditional use of a single timescale (viscoelastic model) cannot account for the detailed shape of $S(Q, \omega)$, and that it only provides guidance for a qualitative description of different dynamical regimes.

Although the effect of an additional timescale in the viscoelastic model has been tested on MD results in the case of rubidium (see page 248 of reference [7]), and theoretical interpretations of such a framework (in particular devoted to the framework of the slow process within mode-coupling theory) have been recently given [23], we give in this work, to the best of our knowledge, the first experimental evidence of the *necessity* of making such an assumption to correctly reproduce the measured $S(Q, \omega)$, stressing the role of the contributions from the different relaxations to $S(Q, \omega)$ in the Q–E regions considered. The presence of a two-timescale mechanism leaves open, however, a point of crucial importance: namely, their physical origin and, most important, that of the fast one.

The slow process, in the terminology used to describe glass-forming systems, is related to the α-relaxation responsible for the liquid–glass transition in systems capable of sustaining strong supercooling. The same process can be framed within kinetic theory in terms of 'correlated collisions': in mode-coupling approaches, the onset of these correlation effects is traced back to the coupling to slowly relaxing dynamical variables and, specifically in the liquid region, to long-lasting density fluctuations. The corresponding decay mechanism (often referred to as 'structural relaxation'), almost negligible in the initial collisional region, controls

† Below Q_m, however, we calculated ω_l from the theoretical classical model adjusted to the experimental data, so that it has the same values on the Stokes/anti-Stokes sides of the spectra.

‡ For a single-component system, such quantities, different on the Stokes/anti-Stokes sides, can be calculated analytically by solving $\partial[\omega^2 S(Q, \omega)]/\partial\omega = 0$. It turns out that $\omega_l(Q) = (\omega_0 \pm \sqrt{\{\omega_0^2 + 8\sigma^2\}})/2$; we solved this equation numerically for the isotopic mixture.

the dynamics at intermediate and long times. For $Q \to 0$ the amplitude of the slow portion of the memory function turns out to vanish as Q^2, whereas at increasing wavevectors it becomes proportional to Q [34]. At sufficiently large Q, the relevance of these couplings as a long-lasting decay channel decreases markedly. In fact, in a rather wide portion of the range of wavevectors explored, we find that the amplitude $\Delta_L^2(Q)$ of the *total* memory function behaves approximately as Q^2. Therefore, outside the hydrodynamic region, the normalized weight of the slowly varying contributions to $M_L(Q,t)$ approximately decreases proportionally to $Q/Q^2 = 1/Q$. This weight may reasonably be identified with the dimensionless amplitude factor $\alpha(Q)$ in the model of equation (16). A quantitative understanding of the 'slow' timescale would require a full evaluation of the mode-coupling contribution at different wavevectors, as was in fact done in the above-mentioned MD study [23].

The situation is much more involved as far as the fast process is concerned and, in fact, its microscopic interpretation is still a matter of debate. In the present work we have given experimental evidence that, in liquid Li, the fast process is indeed the dominant one, and *it is the main controller of both the speed-of-sound dispersion and its attenuation*, i.e. the position and the width of the Brillouin component of the spectra. This observation shows the need for a detailed discussion on the nature of the fast relaxation channel. Within generalized kinetic theory the fast initial decay of both single-particle and collective memory functions is traced back to collisional events, which are short ranged both in space and in time. In particular, in the collective case, the short timescale $1/\gamma_1(Q)$ can be associated with the duration of a rapid structural rearrangement occurring over a spatial range $\simeq 2\pi/Q_m$. In most liquids, at low and intermediate wavevectors, the typical value of the time $1/\gamma_1(Q)$ is of the order of a few 10^{-14} s, with some structural oscillations showing a decreasing trend [35]. At $Q > Q_m$, the structural effects damp out, the decrease becomes more marked and, when the single-particle aspects start to prevail, $1/\gamma_1(Q) \propto Q^{-1}$. An inspection of the results reported in a recent MD study on liquid lithium near melting [23] basically confirms these qualitative features as well as the actual values of the 'short time' found in our data analysis (see figure 7). Although the description of the fast process in terms of interparticle collision is a possible way to account for the dynamical features at short times, it does not provide a deep insight into the physics behind it.

Although the description of the fast process in terms of local collisional events has been widely used in the past to account for the short-time dynamics, other mechanisms cannot be excluded. We have already mentioned in section 2 that a formally similar 'microscopic mechanism' has been introduced in the analysis of the Brillouin spectra of glass formers [25]; more recently, an analogous microscopic relaxation process has been detected in a simulated harmonic glass [36]. Generally speaking, the inclusion of a relaxation process in a memory function reflects the existence of decay channels by which the energy stored in a given degree of freedom ('mode') relaxes toward other modes. The problem is then the physical identification of the modes entering the fast relaxation process, and the ultimate origin of the latter in a widely different class of systems ranging from fluids to glasses. In generalized kinetic theories the mechanism is traced back to a manifold of non-hydrodynamic, phase-space 'kinetic' modes, whose non-conserved character ensures a rapid decay of the memory function [35,37]. A different approach used to describe the fast part of the memory function in disordered systems relies on the normal-mode ('instantaneous' in normal liquids) analysis of the atomic dynamics [38]. In this case one uses a framework (dynamical matrix etc) formally similar to the one customarily adopted for harmonic crystals; however, owing to the lack of translational symmetry of the system, it turns out [36] that the eigenstates cannot any longer be represented by plane waves (PW) even at relatively small wavevectors [39]. As a result, when probing the system at a specific wavevector Q, one effectively detects a transfer from a PW mode toward

other PWs of different wavevectors. Assuming that it is actually this energy flow which causes the fast relaxation, we deal with a mechanism whose ultimate origin is the topological disorder, and not a truly dynamical event. Ordinary liquids (such as the one considered here) are certainly 'disordered systems' and, at the high frequency considered here ($\omega\tau_\alpha \gg 1$), they can be considered as 'frozen'; therefore the description used for glasses can be applied as well. At the present stage of the theory, our experimental data cannot support either interpretation, or even ascertain whether the distinction is largely semantic or not. However, the possibility that the phenomenology reported here for a simple liquid can be understood within the same model framework as was developed for more complex liquids and glasses is certainly interesting. Further studies on other simple fluids, for example neon [40], seem to suggest that this is indeed the case.

Acknowledgments

We gratefully acknowledge the ID-16 (ESRF) beamline staff for assistance during the preparation and performance of the experiments. One of us (T Scopigno) is indebted to Dr R Di Leonardo for many fruitful discussions.

References

[1] Copley J R D and Rowe M 1974 *Phys. Rev.* A **9** 1656
[2] Bodensteiner T, Morkel C, Gläser W and Dorner B 1992 *Phys. Rev.* A **45** 5709
[3] Morkel C and Gläser W 1986 *Phys. Rev.* A **33** 3383
Stangl A, Morkel C, Balucani U and Torcini A 1996 *J. Non-Cryst. Solids* **205–207** 402
[4] Verkerk P, De Jong P H K, Arai M, Bennington S M, Howells W S and Taylor A D 1992 *Physica* B **180+181** 834
[5] Novikov A G, Savostin V V, Shimkevich A L and Yulmetiev R M 1996 *Physica* B **228** 312
[6] Chieux P, Dupuy-Philon J, Jal J F and Suck J B 1996 *J. Non-Cryst. Solids* **205–207** 370
Pasqualini D, Vallauri R, Demmel F, Morkel C and Balucani U 1999 *J. Non-Cryst. Solids* **250–252** 76
[7] Balucani U and Zoppi M 1983 *Dynamics of the Liquid State* (Oxford: Clarendon)
[8] De Jong P H K 1993 *PhD Thesis* Technische Universiteit Delft, Netherlands
[9] De Jong P H K, Verkerk P and De Graaf L A 1993 *J. Non-Cryst. Solids* **156–158** 48
[10] Rahman A 1974 *Phys. Rev. Lett.* **32** 52
Rahman A 1983 *Phys. Rev.* A **27** 3174
[11] Balucani U, Torcini A and Vallauri R 1992 *Phys. Rev.* A **46** 2159
Balucani U, Torcini A and Vallauri R 1993 *Phys. Rev.* B **47** 3011
Kambayashi S and Kahl G 1992 *Phys. Rev.* A **46** 3255
[12] Torcini A, Balucani U, De Jong P H K and Verkerk P 1995 *Phys. Rev.* E **51** 3126
[13] Canales M, Gonzales L E and Padrò J A 1994 *Phys. Rev.* E **50** 3656
[14] Burkel E 1991 *Inelastic Scattering of X-rays with Very High Energy Resolution* (Berlin: Springer)
[15] Burkel E and Sinn H 1994 *J. Phys.: Condens. Matter* **6** A225
[16] Burkel E and Sinn H 1995 *Int. J. Thermophys.* **16** 1135
[17] Sinn H, Sette F, Bergman U, Halcousis Ch, Krisch M, Verbeni R and Burkel E 1997 *Phys. Rev. Lett.* **78** 1715
[18] Sinn H 1995 *PhD Thesis* Universität Erlangen–Nürnberg
[19] Mori H 1965 *Prog. Theor. Phys.* **33** 423
[20] Boon J P and Yip S 1980 *Molecular Hydrodynamics* (New York: McGraw-Hill)
[21] Kubo R and Tomita K 1954 *J. Phys. Soc. Japan* **9** 888
[22] Lovesey S W 1994 *Theory of Neutron Scattering from Condensed Matter* (Oxford: Clarendon) p 120
[23] Casas J, Gonzales D J and Gonzales L E 1999 *Phys. Rev.* B **60** 10 094
Casas J, Gonzales D J, Gonzales L E and Silbert M 1998 *LAM 10 (Dortmund) Preprint*
[24] Levesque D, Verlet J and Kurkijarvi J 1973 *Phys. Rev.* A **7** 1690
[25] Li G, Du W M, Chen X K, Cummins H Z and Tao N J 1992 *Phys. Rev.* A **45** 3867
[26] Verbeni R, Sette F, Krisch M, Bergman U, Gorges B, Halcoussis C, Martel K, Masciovecchio C, Ribois J F, Ruocco G and Sinn H 1996 *J. Synchrotron Radiat.* **3** 62

[27] Masciovecchio C, Bergman U, Krisch M, Ruocco G, Sette F and Verbeni R 1986 *Nucl. Instrum. Methods* B **111** 181
Masciovecchio C, Bergman U, Krisch M, Ruocco G, Sette F and Verbeni R 1986 *Nucl. Instrum. Methods* B **117** 339
[28] Scopigno T *et al* 2000 to be published
[29] Masciovecchio C, Mazzacurati V, Monaco G, Ruocco G, Scopigno T, Benassi P, Cunsolo A, Fontana A, Krisch M, Mermet A, Montagna M, Rossi F, Sampoli M, Scopigno T, Signorelli G and Verbeni R 1999 *Phil. Mag.* **79** 1987
[30] Scopigno T 1997 *Thesis* University of L'Aquila, Italy
[31] *Handbook of Thermodynamic and Transport Properties of Alkali Metals* 1985 ed W Ohse *et al* (Oxford: Blackwell Scientific) p 735
[32] Mountain R D 1966 *J. Res. NBS* A **70** 207
[33] Fioretto D, Buchenau U, Comez L, Sokolov A, Masciovecchio C, Mermet A, Ruocco G, Sette F, Wilner L, Frick B, Ritcher D and Verdini L 1999 *Phys. Rev.* E **59** 4470
[34] Bengtzelius U, Gotze W and Sjolander A 1984 *J. Phys. C: Solid State Phys.* **17** 5915
[35] Sjogren L 1980 *Phys. Rev.* A **22** 2866
Sjogren L 1980 *Phys. Rev.* A **22** 2883
[36] Ruocco G, Sette F, Di Leonardo R, Monaco G, Sampoli M, Scopigno T and Viliani G 2000 *Phys. Rev. Lett.* **84** 5788
[37] de Schepper I M and Cohen E G D 1982 *J. Stat. Phys.* **27** 223
[38] Seeley G and Keyes T 1989 *J. Chem. Phys.* **91** 5581
[39] Mazzacurati V, Ruocco G and Sampoli M 1996 *Europhys. Lett.* **34** 681
[40] Cunsolo A *et al* 2000 *J. Chem. Phys.* submitted